Polymer Chemistry

Accepted Manuscript

ROYAL SOCIETY OF CHEMISTRY

www.rsc.org/polymers

Organophosphonic acids as viable linkers for the covalent attachment of polyelectrolyte brushes on silica and mica surfaces†

Olga Borozenko,[1] Vivian Machado[2], W. G. Skene[1] and Suzanne Giasson[1,2]**

[1]Department of Chemistry and [2]Faculty of Pharmacy, Université de Montréal, C.P. 6128, succursale Centre-Ville, Montréal, QC, Canada, H3C 3J7

* corresponding authors: w.skene@umontreal.ca and suzanne.giasson@umontreal.ca

RECEIVED DATE (to be automatically inserted after your manuscript is accepted if required according to the journal that you are submitting your paper to)

†Electronic supplementary information (ESI) available: synthetic scheme of initiator (**5**), H NMR, C NMR, HR MS spectra of intermediate products and **5**, theoretically calculated length of **5**, AFM images of PAA and PSPMAA brushes grafted from **6** on silica, degrafting studies of PAA brushes synthesized from **5**-modified silica wafer, PAA layer roughness data. See DOI:

TOC

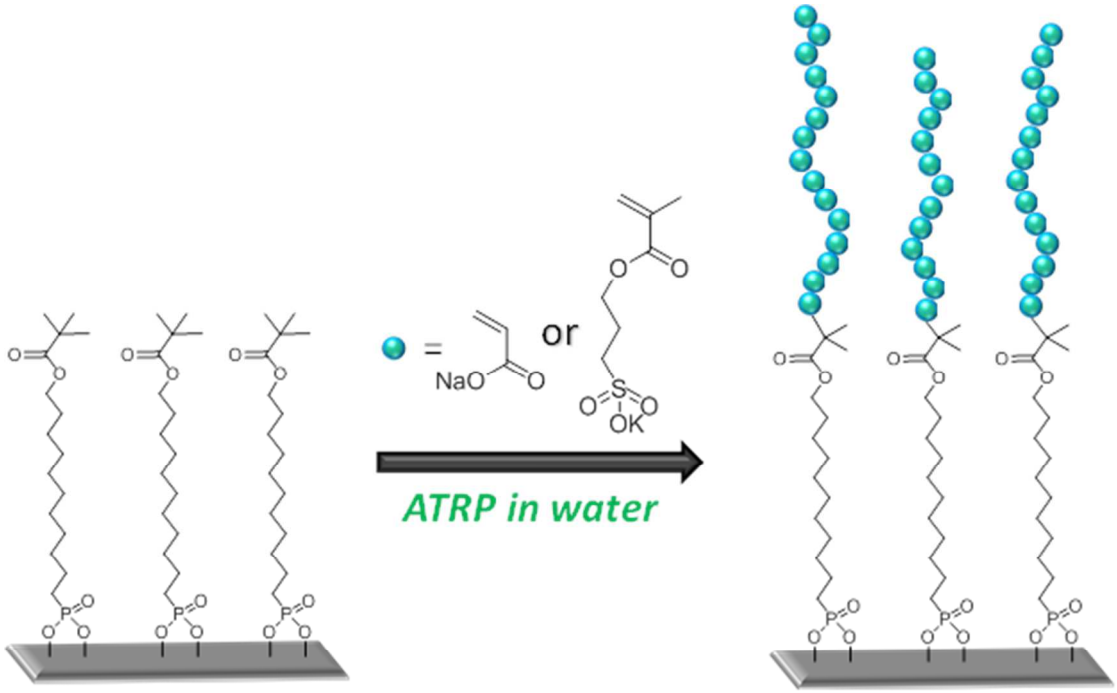

Abstract

We report the first successful preparation of polyelectrolyte brushes using an ATRP initiator that was covalently grafted to silica and mica substrates via an organophosphonic acid. Covalent attachment of the initiator to silica and mica and its subsequent synthesis of polyacrylic acid (PAA) and poly(sulfopropyl methacrylic acid) brushes by water mediated-ATRP was confirmed by ATR-FTIR, ellipsometry, AFM, and contact angle measurements. The initiator–substrate bond was robust and could resist a large range of pH in the absence of salt. Interactions between PAA brushes anchored to mica via the organophosphonic acid initiator were investigated using the Surface Forces Apparatus. The results confirmed the robustness of the initiator–mica bond as the brushes could resist shearing and compression under relatively high applied loads.

Introduction

Grafting of polymer brushes is a particularly versatile way of tailoring the surface properties of materials such as wettability, lubrication, and biocompatibility.[1-3] Polymer brushes are monolayers of polymer chains with one chain end tethered to a surface. Polymer brushes are generally observed for large surface density of grafted chains for which the limited space forces the chains to stretch. The polymer chain conformation depends on the grafting density, molecular weight and chemical composition of the grafted chains.[4] In addition, end-tethered polymer brushes can change their conformation in response to the external trigger such as solvent quality, pH and/or ionic strength.[5] This dynamic behavior is widely exploited for developing smart materials, having tunable surface properties.[3, 6-8] One of the most suitable methods for preparing

polymer brushes having a controlled grafting density and thickness is the *grafting-from* approach. This relies on synthesizing polymers directly from an initiator-modified surface in a well-defined manner.[9] By controlling the initiator surface coverage and the polymer molecular weight, a wide range of polymer grafting densities and chain conformations are possible.[4]

Silicon oxide derivatives are widely used as substrates for synthesizing and characterizing polymer brushes.[10] Silica surfaces have a significant number of silanol groups that can undergo silanization reactions with organosiloxanes.[11] Surface polymerization takes advantage of an organosiloxane initiator monolayer that is covalently anchored to the surface via a Si–O–Si bond.[12, 13] However, the labile siloxane bond between the surface and the initiator is susceptible to hydrolysis, leading to polymer cleavage from silica substrates in aqueous media under extreme pH and ionic strengths.[14, 15] Organophosphonic acids are attractive alternatives to organosiloxanes for anchoring polymers to substrates. This is in part owing to the multiple bonds occurring between organophosphonic acids and various substrates.[16-18] These are expected to give rise to robustly grafted uniform monolayers. Indeed, grafted organophosphonic acids have shown higher stability than siloxanes on metallic surfaces even at pH 7.5 for 7 days.[19] For this reason, organophosphonic acids have also been grafted onto silica surfaces for various purposes such as immobilizing biological molecules,[20, 21] biosensor applications,[22] and organic thin-film transistors.[23-26] Despite their widespread use, only a limited number of studies have investigated the controlled surface polymerization from organophosphonic acid initiators and these exclusively focused on metal surfaces.[27-31] We therefore report the first controlled ATRP of polyelectrolytes using an organophosphonic acid initiator covalently attached to silica and mica substrates. Polyacrylic acid and poly(sulfopropyl methacrylic acid) brushes were examined owing to their known responsiveness to pH and ionic strength. They were additionally targeted

to elucidate the role of brush conformation and electrostatic interactions in controlling adhesion and friction forces between surfaces in an aqueous environment. This is important because the use of dense end-grafted polyelectrolyte brushes has often been proposed for their remarkable lubricating properties. However, the role of the polymer's conformation and its degree of ionization in controlling friction remains unclear.[2, 32-34] Water-mediated ATRP was chosen because it is fast, straightforward, and compatible with the targeted hydrophilic monomers.[35] In addition, the desired polyelectrolytes can be prepared without additional experimental conditions and organic solvents that otherwise are incompatible with accurate surface measurements using a Surface Forces Apparatus (SFA). Herein, we demonstrate as a proof-of-concept that the organophosphonic acid (**5**, Scheme 1) is a viable alternative to its siloxane derivative for the ATRP of polyelectrolytes that are covalently grafted on both silica and mica substrates.

Experimental section

Materials and chemicals. Silicon wafers were obtained from University Wafer Co (100-mm diameter, boron-doped, (100) orientation, one side polished). All chemicals were used as received from Aldrich unless specified. Copper bromide (CuBr) was purified according to the previous report.[36] MilliQ water was obtained from Millipore A10 purification system with a resistivity of 18.2 MΩ·cm at 25° C. All surface manipulations were performed under an air flow cabinet and all glassware was carefully cleaned and oven-dried at 120^{o} C overnight.

Synthesis

11-(2-Bromoisobutyrate)-undecyl-1-phosphonic acid was synthesized in five steps similarly to previously reported method (see Figure S1 for synthetic scheme).[27]

11-Bromo-1-(tetrahydropyranyloxy)undecane (1). In a 100 mL round-bottom flask equipped with a stir bar, 11-bromoundecanol (3.3 g, 13.1 mmol) and a catalytic amount of *p*-toluenesulfonic acid (15 mg, 0.09 mmol) were mixed in dichloromethane (15 mL) at room temperature. The flask was then immersed in an ice bath at 0°C and an excess of 3,4-dihydro-2H-pyrane (6 mL, 65.7 mmol) was added drop-wise. After stirring the reaction mixture at room temperature for 73 h, diethyl ether (20 mL) was added. The ethereal layer was washed 3 times with a saturated sodium chloride aqueous solution. It was then dried over $MgSO_4$, filtered, and concentrated under reduced pressure. The crude product was purified by column chromatography (silica gel, eluent – hexane:ether=10:1, stained by vanillin or PMA). The title compound was isolated as a yellowish liquid (3.6 g, 81 %). ^{1}H-NMR (400 MHz, $CDCl_3$): δ 1.28‑1.42 (m, 18H), 1.54-1.59 (m, 6H), 3.41 (m, 2H), 3.5 (m, 2H), 3.72 (m, 1H), 3.87 (m, 1H), 4.57 (dd, 1H). MS (ESI) m/z calculated 359 ($[M+Na+H]_+$); found 359.

11-(Diethylphosphoryl)-1-(2-tetrahydropyranyloxy)-undecane (2). In a 100 mL double-neck round-bottom flask fitted with reflux condenser was loaded with **1** (3.6 g, 10.7 mmol). It was then closed with a septum and triethyl phosphite (30 mL, 175 mmol) was added. The reaction mixture was stirred at 165° C for 48 h. Afterwards, the triethyl phosphite excess was removed by vacuum distillation at 40° C at 4 x 10^{-2} mm Hg. The title compound was obtained as a yellowish liquid (1.46 g, 35 %). ^{1}H NMR (400 MHz, CDCl3): δ 1.25‑1.30 (m, 24H), 1.57 (m,2H), 1.70 (m, 6H), 3.35-3.37 (m, 1H), 3.85 (m, 1H), 4.08 (m, 4H), 4.56 (dd, 1H). ^{13}C-NMR

(100 MHz, CDCl3): δ 98.8, 77.4, 77.1, 76.7, 67.7, 62.4, 61.4, 61.3, 30.8, 30.7, 30.5, 29.8, 29.6, 29.5, 29.4, 29.1, 26.3, 25.5, 25.0, 19.7, 16.5. MS (ESI) m/z calculated 415 ($[M+Na]^+$); found 415.

11-(Diethylphosphonyl)-undecanol (3). **2** (1.46 g, 3.7 mmol) and pyridinium-*p*-toluene-sulfonate (PPTS; 50 mg, 0.2 mmol) were combined in a 50 mL two-necked flask along with In methanol (15 mL) . The reaction mixture was refluxed at 60° C for 48 h. Afterwards, the mixture was cooled to room temperature and dichloromethane (20 mL) was added. The organic layer was washed 3 times with a saturated sodium chloride aqueous solution. It was then then dried over $MgSO_4$, filtered, and concentrated under reduced pressure. The title compound was isolated as a yellowish liquid (1.1 g, 96 %). ^{1}H NMR (400 MHz, CDCl3): δ 1.26‑1.30 (m, 24H), 1.54 (m, 2H), 3.62 (t, 2H), 4.08 (m, 4H). ^{13}C-NMR (100 MHz, CDCl3): δ 77.4, 77.1, 76.7, 63.0, 61.4, 32.8, 30.7, 30.5, 29.5, 29.4, 29.3, 26.4, 25.7, 25.0, 22.4, 16.5. MS (ESI) m/z calculated 309 ($[M+H]^+$); found 309.

11-(2-Bromoisobutyrate)-undecyl-1-diethylphosphonate (4). In a 100 mL round bottom flask was loaded **3** (1.1 g, 3.6 mmol), anhydrous THF (10 mL), and an aqueous pyridine solution (99.5%; 1 mL, 12.4 mmol). 2-Bromoisobutyryl-bromide (1.2 mL, 9.7 mmol) was dissolved in THF (5 mL) and then it was added dropwise to the reaction mixture over 5 min. The reaction mixture was then stirred overnight at room temperature. Afterwards, petroleum ether (20 mL) was added and the organic layer was washed 3 times with 2 M HCl aq, twice with water, and twice with a saturated sodium chloride aqueous solution. The organic layer was extracted, dried over $MgSO_4$, and filtered. The solvent was removed under reduced pressure and the resulting oil was purified by column chromatography (silica; hexane:ethyl acetate=1:9; stained

with $KMnO_4$). The title compound was isolated as a yellow oil (0.6 g, 38 %). ^{1}H NMR (400 MHz, CDCl3): δ 1.31 (24H), 1.67 (m, 2H), 1.92 (s, 6H), 4.08 (m, 4H), 4.16 (t, 2H). ^{13}C-NMR (100 MHz, CDCl3): δ 171.8, 66.2, 61.5, 56.0, 30.8, 29.4, 29.1, 28.4, 26.4, 25.8, 24.9, 22.4, 16.5. MS (ESI) m/z calculated 459 ([M+2H]+); found 459.

11-(2-Bromoisobutyrate)-undecyl-1-phosphonic acid (5). A 50 mL round-bottom flask was loaded **4** (0.6 g, 1.3 mmol), afterwards bromotrimethylsilane (0.1 ml, 0.76 mmol) was added dropwise. The reaction mixture was stirred overnight at room temperature and then it was quenched with acetone/water (4/1) mixture. The excess acetone was removed under reduced pressure and the final product was isolated as a yellow powder (475 mg, 1.18 mmol, 90 %). ^{1}H NMR (400 MHz, CDCl3): δ 1.3 (m, 18H), 1.7 (m, 2H), 1.95 (s, 6H), 4.19 (t, 2H). ^{13}C-NMR (100 MHz, CDCl3): δ 171.9, 77.4, 77.0, 76.7, 66.2, 57.7, 56.0, 30.8, 29.5, 28.4, 25.8, 25.7, 21.6. MS (ESI) m/z calculated 403 ([M+2H]+); found 403. HR-MS (ESI) m/z calculated 403 ([M+2H]+); found 403.

Substrate preparation and initiator immobilization

Silicon wafers. Silicon wafers were cut into 1x2 cm^2 pieces using a diamond pencil, sonicated in acetone for 20 min and then dried under nitrogen. The substrates were activated using a Piranha solution (H_2SO_4(conc.):H_2O_2=70:30 v:v) for 20 min at room temperature. (Caution: Piranha solution is extremely corrosive and should be used with absolute carefulness!) Afterwards, the substrates were removed from the Piranha solution and they were washed with copious amounts of MilliQ water, absolute ethanol, and finally dried thoroughly under nitrogen. The ATRP initiator (**5**) was solubilized in anhydrous dichloromethane (vide infra) at a

concentration of 10^{-2} M. The clean substrates were immersed into the initiator solution overnight at room temperature under argon. They were then removed from the solution, washed with dichloromethane, and sonicated for 15 min in a triethylamine solution (2 mM) in dichloromethane. Afterwards, the surfaces were rinsed with dichloromethane, dried under nitrogen, and finally annealed at 140°C for 3 h in the oven. The phosphonic acid initiator (**5**) modified surfaces were subsequently either used for ATRP polymer grafting or stored in at desiccator under an inert atmosphere.

SFA samples. Back-silvered mica pieces were glued silver side down to SFA silica discs using an optical adhesive (Norland Products Inc., USA). The prepared surfaces were treated with a H_2O/Ar plasma (total pressure of 300 mTorr) to generate an active mica silanol surface.[37] After plasma activation, the disks were immediately transferred into a compartmentalized flask filled with the phosphonic acid initiator solution in anhydrous THF at a concentration of 10^{-2} M. The substrates were then removed from the solution, soaked in 2 mM triethylamine solution in THF for 30 min, rinsed with THF, dried under a steam of nitrogen, and finally annealed at 140°C for 3 h. Afterwards, the **5**-modified SFA samples were used for surface initiated (SI) ATRP of sodium acrylate (NaA).

5 recycling. The excess **5** used in the grafting solutions was isolated and reused several times without any detrimental effect either on the grafting or polymerization. A 50 mL round-bottom flask containing the **5** solution was closed with a septum and the solvent was evaporated under a stream of argon until dry. The product was stored in the same flask under argon. The product stability and structural integrity were confirmed by HR-MS (Figure S17).

Synthesis of conventional ATRP initiator and its grafting to silica. The ATRP initiator, 3-(chlorodimethylsilyl)propyl-2-bromoisobutyrate (**6**) was synthesized according to previous reports.[36] Piranha-treated silicon substrates were exposed to a 10^{-3} M initiator solution in toluene for overnight at room temperature under nitrogen.[36] Afterwards, the initiator-covered surfaces were washed with toluene, absolute ethanol, and finally dried under a steam of nitrogen. The freshly prepared initiator-functionalized silica substrates were either used for surface-initiated polymerization or stored in a desiccator until used.

Synthesis of polyacrylic acid (PAA) and poly(3-sulfopropyl methacrylic acid) (PSPMAA) brushes via ATRP from initiator-functionalized silica and mica surface. A typical polymerization from the initiator-modified substrate (silica or mica) was as follows: bipyridine (129 mg, 0.83 mmol) and CuBr (48 mg, 0.33 mmol) were mixed in 100 mL double-necked round bottomed flask and the mixture was deoxygenated under vacuum and backfilled with argon three times. $CuBr_2$ (15 mg, 0.07 mmol) was added to the mixture and three vacuum-argon cycles were performed. Sodium acrylate (NaA) (9 g, 95.7 mmol) or 3-sulfopropyl methacrylate potassium salt (KSPMA) (23.5 g, 95.7 mmol) was solubilized in milliQ water (15 mL) along with methanol (3 mL) at room temperature. The resulting solution was degased for 30 min by purging it with argon. The monomer was transferred to the catalyst mixture and the mixture was stirred at 50^{o} until a homogeneous brown solution was obtained. The initiator-bearing substrates (maximum 4) were placed into an oven-dried compartmentalized flask, which was deoxygenated under vacuum and backfilled with argon three times. The monomer/catalyst solution was then transferred to the compartmentalize flask by cannula. Polymerization was done

for 1 h at room temperature. The reaction was stopped by opening the flask and exposing the catalyst to air. The substrates were removed, soaked in milliQ water for overnight (> 8 h), and then soaked in ethanol for 1 h followed by drying under nitrogen. Under these conditions, the salt is converted to the corresponding acid.

PAA degrafting/swelling studies. Trizma base buffer solutions (0.1 M) were prepared with MilliQ water and the pH was adjusted to 7.5, 9.0, 9.5, 10.0 and 10.5 with different volumes of HCl (0.1 M). The pH was measured with a Symphony SB20 pH meter with Ag/AgCl electrode. The ionic strength was adjusted by adding NaCl (10 mM) to the Trizma buffer solution.

Surface Characterization

Contact Angle Measurements. The water wettability of initiator- and polymer-covered substrates was measured with a FTA200 dynamic contact angle analyzer (First Ten Angstrom) in the equilibrium static mode using MilliQ water as the probe liquid. Fta32 Video software was employed for data analyses. At least three separate measurements were done for each substrate and the average contact angle value was determined within an error of $\pm 3^{o}$.

AFM measurements. All surface topographical studies in air (unless specified) were performed using a MultiMode microscope equipped with a NanoScope V extended controller (Digital Instruments, Santa Barbara, CA) at room temperature with a constant humidity $\leq 40\%$. The surfaces were imaged in a tapping-mode using an ACTA silicon probe tip from AppNano

with a resonance frequency of ~300 kHz and a spring constant of 40 N/m. All dry images were obtained at 1 kHz scan rate, medium oscillation damping (15–20%) and resolution of 512 x 512 pixels. NanoScope 7.30 software was used to treat the images. A minimum of three different areas were analyzed for each surface.

All AFM images in liquid were recorded using a Dimension 3100 MultiMode Scanning Probe Microscope equipped with Veeco NanoScope V extended controller (Digital Instruments, Santa Barbara, CA) by using HYDRA-All-G silicon nitride probes tip A or B. Triangular tip A with a resonance frequency of ~66 kHz and a spring constant of 0.29 N/m was used for imaging the polymer-coated surfaces at pH 9.5 and 10.5. Tip B with a resonance frequency of ~17 kHz and a spring constant of 0.045 N/m was used at low pH (5.5-8.5). A sample was fixed inside a custom-made Teflon liquid cell, filled with buffer solution, and left to equilibrate for at least 2 h before scanning. All images were done in the tapping mode at 1 kHz scan rate with an image resolution of 512 x 512 pixels and weak oscillation damping (10-15%). NanoScope 7.30 software was used to treat the images. A scratch on the polymer layer was made by using a scalpel and the height difference between bare substrate and an outer layer of the polymer film was measured by step-height analysis at three different regions for each sample.

Spectroscopic ellipsometry. The thickness of the initiator- and polymer-coated silica substrates was measured using an Ellipsometer M2000V from J.A.Woollam Co at a 75° angle of incidence at room temperature in air. The wavelength range from 370 to 1000 nm was used. Three different spots were analyzed for each sample. The modeling and data fitting were performed using the WVASE32 software (J. A. Woollam Co, version 3.768). A 2 nm (±0.03 nm) thick silicon oxide layer was measured prior to surface modification and it was considered as a

constant when modeling the initiator and polymer layers using the Cauchy layer, assuming transparent and homogeneous polymer films.

Fourier Transform Attenuated Total Reflection Infrared Spectroscopy (ATR-IR). ATR infrared spectra of the initiator- and polymer-modified silicon wafers were recorded with a Tensor 27 Bruker Optics spectrometer equipped with a Harrick Seagull accessory. A germanium ATR crystal was used with p-polarized light at an incidence angle of 60^{o}. The spectra were compile from 1024 scans at a resolution of 4 cm^{-1}.

Forces measurements with SFA. The surface forces technique (SFA) and detailed experimental procedures for measuring the normal and friction forces are described elsewhere.[38-41] In brief, two back-silvered molecularly smooth mica surfaces are glued to cylindrically curved silica lenses of radius R=2 cm. The force−distance profile between the surfaces is obtained by changing the position of the lower surface using a nanopositioner and measuring the actual variation in the separation distance between the surfaces with an interferometry technique using Fringes of Equal Chromatic Orders (FECO) with subnanometric resolution. The interaction force is then determined from the deflection of the spring by using Hooke's law. The upper surface is mounted on a motor-driven sliding device allowing lateral motion.[40, 41] Shearing cycles are carried out by moving the upper surface at constant velocity over a certain distance after which the driving direction is reversed. The upper surface is connected to a vertical cantilever spring whose lateral deflection, allowing the friction force to be determined, is measured using strain gauges with an accuracy of $\pm 10^{-3}$ mN.

RESULTS AND DISCUSSION

Initiator grafting to silica and mica

The rationale for pursuing an organophosphonic acid (**5**) as an ATRP initiator immobilized on silica substrates was to demonstrate that functional groups other than siloxyl derivatives could be used for controlled surface polymerization of polyelectrolytes. This is of importance given the limited number of examples demonstrating the viability of alternate functional groups for the covalent immobilization of *grafted-from* polymers on silica substrates. Organophosphonic acids are advantageous over commonly used trialkoxy silyl counterparts because they consistently form monolayers without stringent deposition protocols. The organophosphonic acid derivative (**5**) was prepared as a proof-of-concept to demonstrate that it could sustain ATRP while being covalently attached to silica substrates. The targeted **5** was prepared by expanding upon known methods, starting from commercially available 11-bromoundecanol.[27] The hydroxyl of 11-bromoundecanol was protected by attaching 2-tetrahydropyranyl group with the presence of catalytic amount of *p*-toluenesulfonic acid. The yield of the protected product **1** was 81%. Nucleophilic displacement of the bromide of **1** by diethyl phosphonate was done in 35% yield. The obtained **2** was deprotected to afford **3** in 96% yield. Next, 2-bromoisobutyryl was introduced to **3** in 38% yield. For the last step, the diethyl groups were removed to afford the final product **5** in 90% yield and 9% overall yield for the five steps.

Owing to the reduced reactivity of silica surfaces towards organophosphonic acids compared to metal oxides, a modified aggregation and growth ("T-BAG") method was used for grafting the initiator to the substrate.[42] This was used as an initial grafting protocol because of

the limited number of studies of organophosphonic acid grafted to silica and mica substrates.[21, 43] The given surfaces were immersed into either a 10^{-3} M dichloromethane or THF solution of **5** overnight (Scheme 1). The substrates were then cleaned in triethylamine solutions of DCM and THF by sonication. This was done to ensure the formation of only a monolayer. The substrates were finally annealed thermally at 120-140^{o} C for 3 h to ensure covalent bonding of the targeted **5** to the substrate.[42]

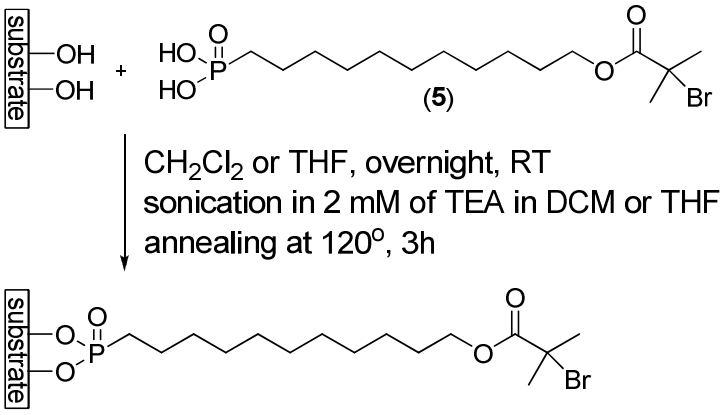

Scheme 1. Schematic representation of the immobilization of the organophosphonic acid initiator studied on a silica surface.

The resulting **5**-modified surfaces were characterized by water contact angle, ellipsometry, ATR-FTIR, AFM measurements. Water contact angles of 65^{o} and 62^{o} were observed for the initiator-modified silica and mica, respectively (Table 1). Meanwhile, an initiator film thickness of 0.9 nm (Table 1) was measured by ellipsometry. The measured contact angles were similar to previously reported values for alkylsilane initiator-modified substrates bearing an identical initiating group. The large contact angles measured confirm the increased hydrophobicity of the surface upon grafting of **5**. This suggests that the initiator is coupled to the substrate, especially

when comparing the contact angle to Piranha treated native glass slides whose θ=0.[14] Unequivocal evidence of chemical bonding of **5** to the SiO_2 substrate was provided by ATR-FTIR. Measurements were done after sonicating the initiator-coated substrate in triethylamine solutions in DCM. This step was to remove any physisorbed initiator. Immobilization of **5** on silica was confirmed by comparing its spectra to an authentic powder sample of **5** that was not attached to a surface (Figure 1). The decrease in the signal between 930 and 955 cm^{-1}, corresponding to the P–OH stretching, and the presence of vibrations from PO_2^- groups at 1072-1048 cm^{-1} observed on **5**-modified silica confirm covalent attachment of **5** to the silica substrate.[44]

Table 1. Film thickness and water contact angle of **5**-modified substrates and polymer brushes.

Substrate	Thickness, nm[a]	Contact angle, degrees [o a]
5-modified silica	0.9±0.2[b]	65±3
5-modified mica	-	62±3
PAA brushes on 5-modified silica	17±4	25±3
PSPMAA brushes on 5-modified silica	13±4	30±3

Concentration of the grafting solution of **5** is 10^{-2} M.

[a] Results are the mean from three different samples ± standard deviation.

[b] The thickness was measured by ellipsometry in air after the sonication step.

ATR-FTIR was further beneficial for providing information about the surface packing. It is well known that the position of the methylene peak correlates with the degree of ordering of the alkyl chains in the film.[45-47] The asymmetric CH_2 stretching of disordered chains usually occurs at higher wavenumbers (~2925 cm^{-1}) than that of well-ordered chains (~2915 cm^{-1}). Figure 1A shows the different relative intensity of the two characteristics CH_2 peaks for **5** in powder and immobilized **5**. After immobilizing the initiator on silica, the CH_2 stretching

dominates at higher wavenumbers, suggesting a weak organization and alignment of the alkyl chains on the surface. This can be attributed to the bulky 2-bromo-2-methylpropionyloxy groups that prevent the layer from forming a close packed arrangement.[27]

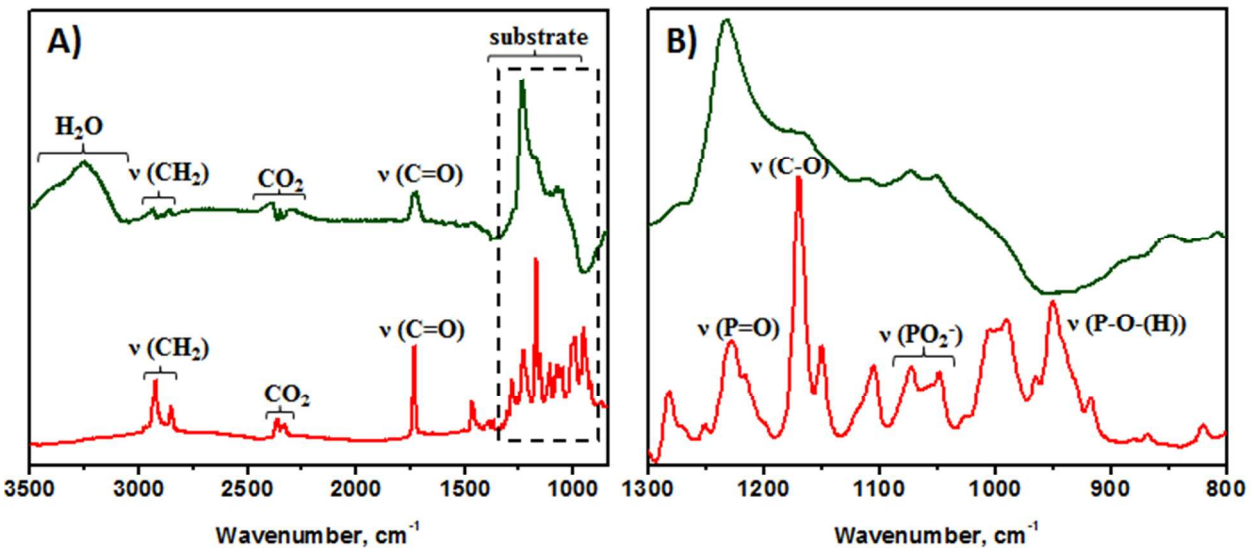

Figure 1. A) ATR-FTIR spectra of **5** as a powder (red line) and immobilized on silica (dark green line). The ATR-FTIR spectrum of bare silica was subtracted from the spectrum of the immobilized **5**. B) Expanded region corresponding to the dashed line from (A).

Figure 2 illustrates the surface topography of the **5**-modified silica (A2, A3) and mica (B2, B3) surfaces. Randomly-distributed particles-like structures having a relative height of ca. 3 nm can be observed on both substrates. Since the length of a fully extended **5** is 2.05 nm (Figure S18), the observed particle-like structures most probably correspond to initiator aggregates on the surface. However, the overall low surface roughness measured by AFM (rms of 0.4 for silica and 0.2 nm for mica) suggests a relative homogeneous grafted initiator layer.

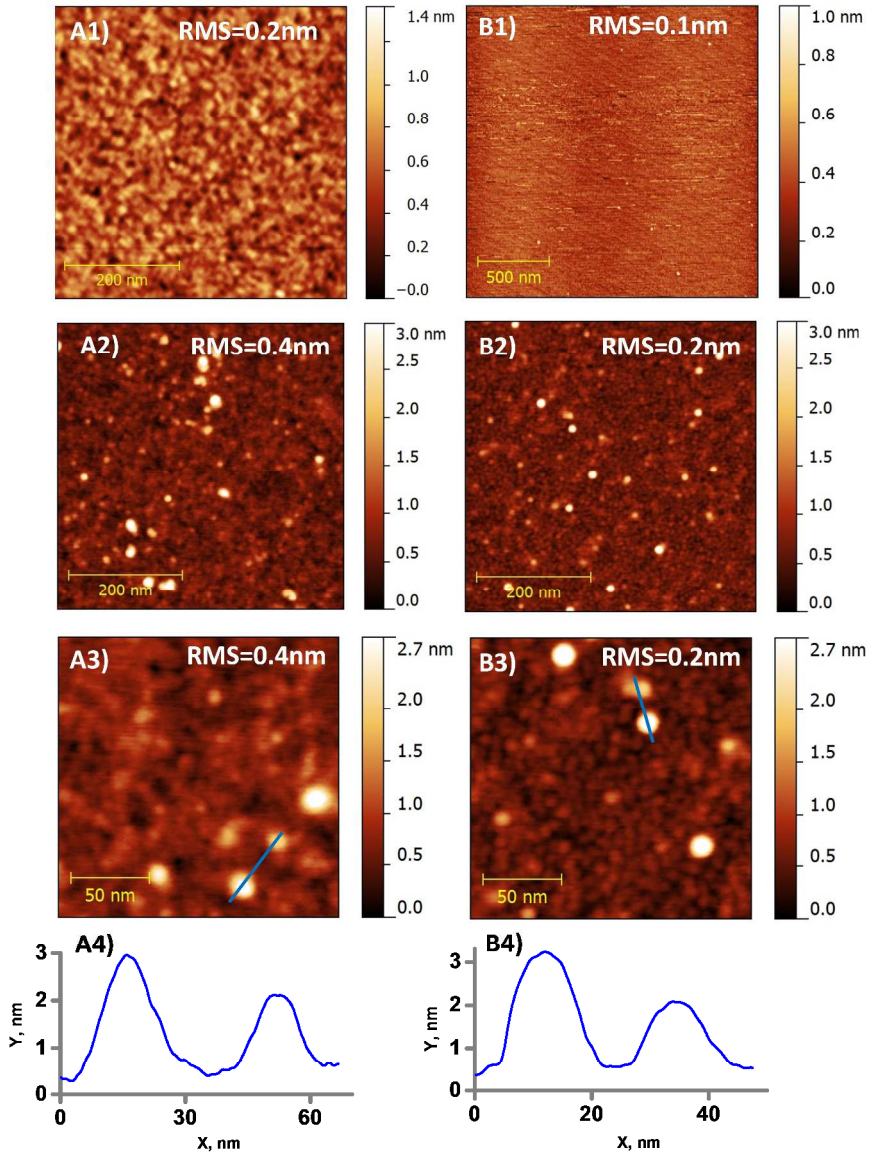

Figure 2. AFM images of native silica (A1 (0.5x0.5 um)) and native mica (B1 (2x2 um)), **5**-modified silica (A2 (0.5x0.5 um), A3 (1.75x1.75 um)), and **5**-modified mica (B2 (0.5x0.5 um), B3 (1.75x1.75 um)). AFM images (A2, A3, B2, B3) were obtained with SmartSPM (AIST-NT Inc, Novato) in the semicontact mode and Hi-Res C -14/Cr-Au probes (Mikromasch). All images were done in air.

ATRP of immobilized organophosphonic acid initiator.

The capacity of **5**-immobilized on silica to initiate the polymerization of different monomers was confirmed by synthesizing polyacrylic acid sodium salt (NaPAA) and poly(3-sulfopropyl methacrylic acid) potassium salt (KPSPMAA) polyelectrolyte brushes (Scheme 2). The ATRP of NaA and KSPMA using the **5**-modified silica wafer was done in water at room temperature using a CuBr/Bipyridine catalyst. A $CuBr_2$ to CuBr ratio of 1:5 was used to moderate the polymerization. This ratio was found to be optimal for fast polymerization and for forming films of sufficient thickness for accurate swelling studies. They were characterized by ellipsometry, ATR-FTIR, AFM and contact angle measurements. After polymerization, the water contact angle of the coated substrates decreased and the grafted layer thickness increased, compared to the original **5**-immobilized substrates (Table 1).

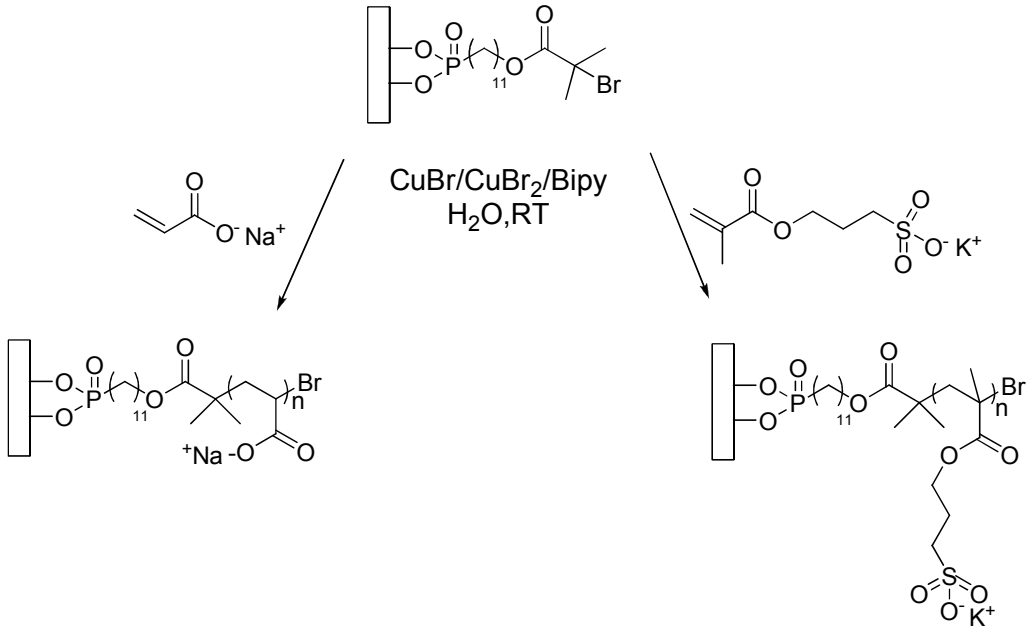

Scheme 2. Schematic representation of the preparation of NaPAA and KPSPMA brushes from surface immobilized **5**.

The resulting polyelectrolyte brushes were converted to their corresponding acid form (COOH) by washing the surfaces with MilliQ water (vide supra) as confirmed by ATR-FTIR. The ATR-FTIR spectra of the PAA showed a strong signal at 1575 cm^{-1}, corresponding to COO^- (Figure 3). Also, the broad peak at 1730 cm^{-1} indicates the presence of hydrogen-bonded carboxylic acids, consistent with previous reports for similar PAA brushes.[48] The presence of both COO- and COOH bands confirms the partial ionization of the carboxylic acid groups. Similarly, the FTIR spectrum of the PSPMAA brushes clearly showed a narrow band at 1730 cm^{-1}, corresponding to the carbonyl. Meanwhile, the sulfonate was confirmed by the two strong peaks at 1195 and 1050 cm^{-1}. These correspond to the asymmetric and symmetric sulfonate stretches.[49]

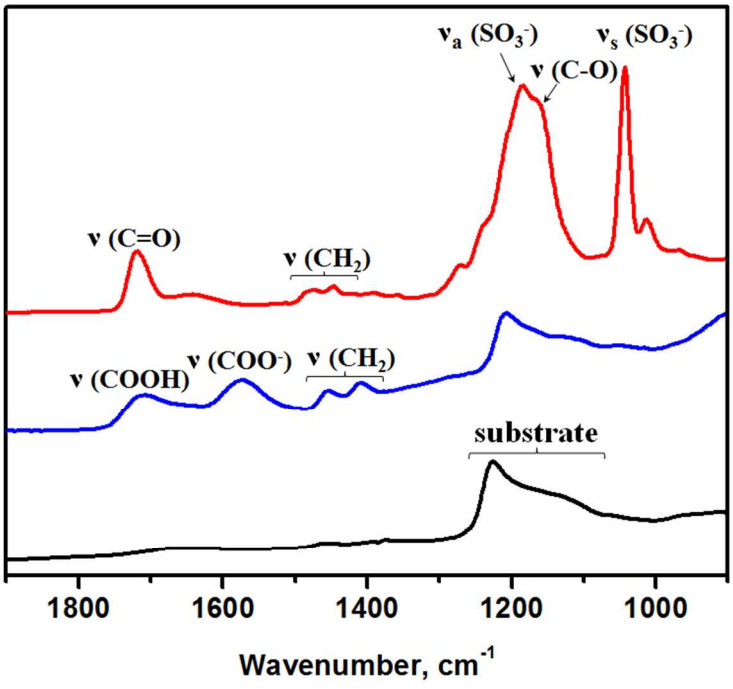

Figure 3. ATR FTIR spectra of PSPMAA (red) and PAA (blue) layers immobilized on silica (black) substrates. PAA and PSPMAA layer thickness= 20 and 13 nm, respectively.

The thickness of the polymerized films was quantitatively determined by ellipsometry. An average dry polymer layer thickness of 17 nm for PAA and 13 nm for PSPMAA was measured after 1 h of polymerization (Table 1). Both the PAA and PSPMAA layers were smooth with a rms of 0.4 nm (Figure 4 A1-A3) and 0.9 nm, respectively (Figure 4 B1-B3). It should be noted that significant differences in the polymer layer thickness were obtained when polymerizing the same monomer with identical polymerization conditions with immobilized **5** and **6**. While both have the same initiator (bromoisobutyrate), the aliphatic chain separating the surface-bound and polymerizable ends of **5** is longer than **6**. Using similar polymerization conditions and an initiator concentration of 10^{-3} M for the surface functionalization, a dry PAA thickness of 2 nm and 120 nm (Figure S19, A) was measured for silica surfaces coated with **5** and **6**, respectively. The different thickness can be attributed to the different initiator surface coverage (Figure 5). Since **6** has a shorter aliphatic segment than **5**, it is expected to form a denser monolayer, resulting in a higher amount of initiating sites on the surface. We previously showed that an increase in initiator coverage is associated with an increase in water contact angle.[14, 15] An increase in concentration of the grafting solution of **5** (from 10^{-3} to 10^{-2} M) also resulted in an increase in the contact angle (from ca 60 to ca 65 ^{o}) as well as an increase in brush thickness (from 2 to 19 nm). Therefore, the smaller contact angle measured for the **5** –covered silica (60 ± 3^{o}) compared to **6**-covered silica (72 ± 3^{o}) for the same initiator concentration (10^{-3} M) suggests a difference in the initiator surface coverage. This can explain the difference in the resulting brush thickness.

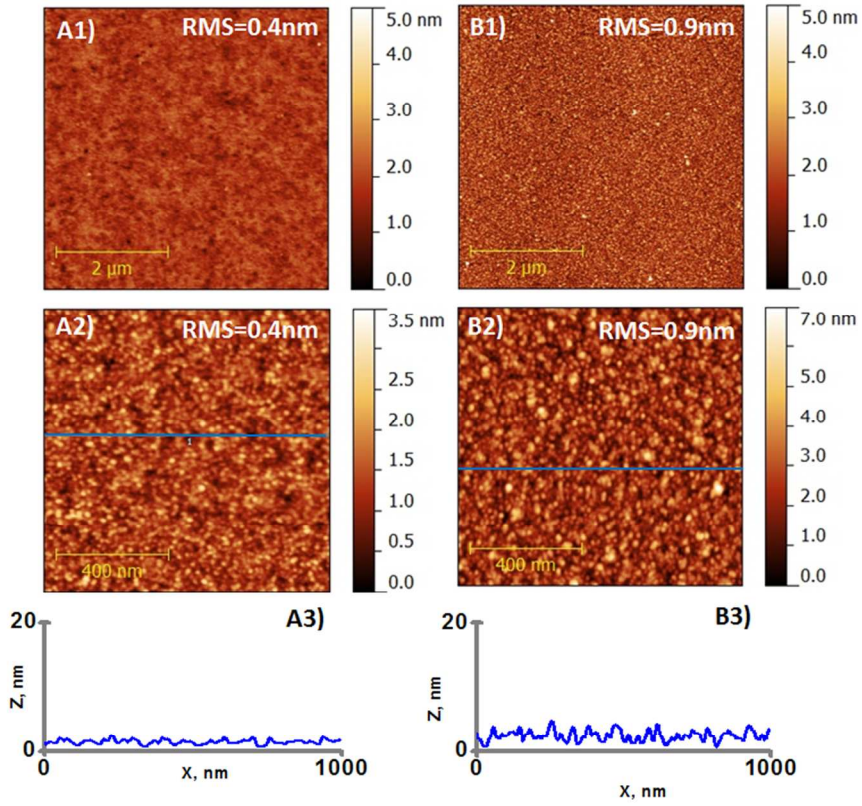

Figure 4. AFM images (A1 (5x5 um), A2 (2x2 um)) and surface topographical profile (A3) of PAA brushes grafted from **5**-functionalized silica. PAA film thickness=15 nm. AFM images (B1 (5x5 um), B2 (2x2 um)) and surface topographical profile (B3) of PSPMAA brushes grafted from **5**-functionalized silica. PSPMAA film thickness=14 nm. All images were done in air.

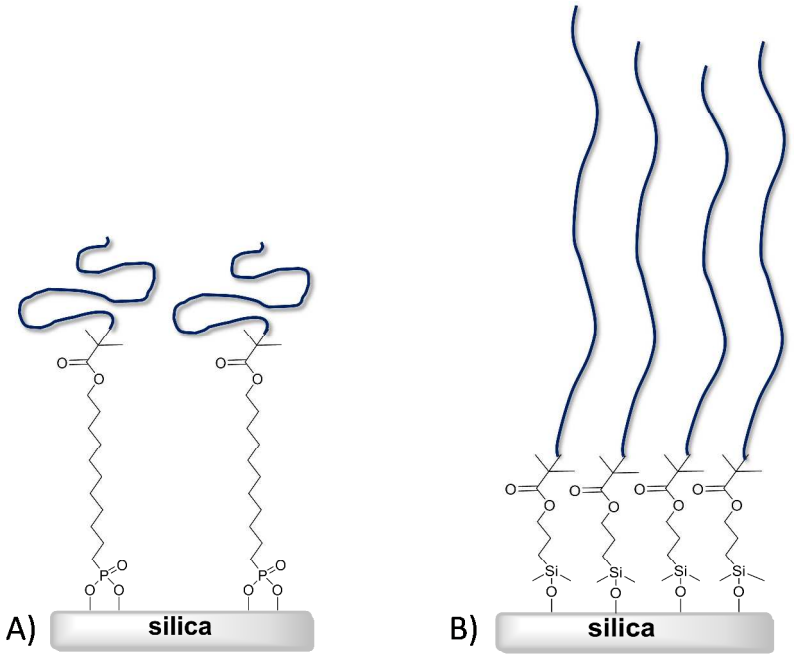

Figure 5. Schematic representation of polymer brushes grafted from **5**- (A) and **6**- (B) immobilized on a silica substrate.

Hydrolytic stability of PAA brushes grafted from silica immobilized 5 and 6.

The stability of the substrate–initiator bond was investigated with PAA brushes polymerized with the silica immobilized **5** and **6** under similar polymerization conditions. The brush swelling and grafting robustness were assessed by measuring the brush thickness at different pH and ionic strength using the AFM step-height method. The thickness of the PAA layer grafted from **6** progressively decreased with increasing pH from 7.5 to 10.0 in the absence of salt (Figure 6). The PAA thickness decrease can arise from either polymer collapse or polymer detachment from the surface. Polymer collapse can be dismissed because the PAA brush was previously demonstrated to swell with increasing pH for this process.[15] This swelling behavior is also confirmed experimentally[15, 50, 51] and predicted by theory[52] for weakly charged polyelectrolyte brushes. Therefore, the decrease in PAA thickness is most probably due to

polymer degrafting. This is in contrast to previous studies that reported no PAA degrafting from silica immobilized derivatives of **6** in salt-free solutions at pH between 5.5 and 10.5.[14, 48] Different PAA degrees of ionization and initiator coverage resulting from different experimental conditions can account for the observed discrepancy. The polymerization conditions used for water-mediated ATRP (pH 8.5) favor the ionization of the carboxylic acid to its carboxylate, whereas the PAA brushes obtained in non-aqueous-mediated ATRP are expected to be neutral.[14, 48] Indeed, a previous report confirmed no PAA brush swelling at pH < 7.5, regardless of the initiator surface coverage, when the brush was prepared in organic solvents using siloxane initiator-covered silica.[48] This behavior was explained by the initial hydrophobicity of the PAA brushes prepared in organic solvents that block water and ions from penetrating the brush that would otherwise cleave the substrate–initiator bond. On the other hand, PAA brushes prepared in aqueous-media are significantly swollen at pH 7.5 (Figure 6A). They are therefore more permeable to water and ions and favor hydrolysis of the substrate–initiator bond. The behavior of the PAA brush prepared from the immobilized-**5** is different from that of the immobilized-**6** (Figure 6). For the immobilized-**5**, the brush thickness remained constant between pH 7.5 and 9.0 and increased at pH 10.0, regardless of the ionic strength. This suggests a more stable substrate–**5** bond compared to its substrate–**6** counterpart under similar polymerization conditions. At higher pH (10.5), the PAA layer thickness slightly increased in salt-free solutions, whereas it drastically decreased in the presence of 10 mM NaCl (Figure 6B, S20). Polymer cleavage was reported for PAA prepared from immobilized-**6** at similar pH and with added salt.[14, 48] It was shown, theoretically and experimentally, that salt can promote the dissociation of the carboxylic acids.[50, 52] This leads to highly stretched chains that are hydrated, making the substrate–initiator more susceptible to hydrolysis by hydroxyl ions, and ultimately, polymer detachment.[14, 48] Even

though numerous stimuli-sensitive polyelectrolyte brushes studies have been reported, the exact swelling responses of PAA brushes and the conditions leading to their cleavage from the surface remain unclear. This is in part owing to the lack of systematic control of the initiator grafting density and molecular weight of the brushes between different analyzed samples. Nevertheless, our comparative study (Figure 6) clearly shows the resistivity of the substrate–**5** bond towards hydrolysis over a large range of pH, especially in the absence of salt, compared to the substrate–**6** bond. The stability of the substrate–initiator bond was theoretically evaluated using Density Function Theory. This was done by calculating the bond dissociation enthalpy (BDE) of the substrate–initiator bond, using the heats of formation (ΔH_f) of the corresponding compounds. The BDE was calculated according to: [ΔH_f(substrate–initiator) + $\Delta H_f(H_2O)_n$] - [ΔH_f(substrate) + ΔH_f (initiator)], where n= 1 for **6** and n=2 for the bidentate bonding for **5** to the surfaces. $Si(OH)_4$ was used as a representative model for the silica substrate to significantly reduce the computational times. This simplification is valid given only the relative BDE of the substrate-initiator are targeted and not the absolute values. Gas phase geometric optimization was done using the 6-31g* basis set. Single point energies and the corresponding ΔH_f of the optimized geometries were calculated by applying a given solvent continuum. While the absolute ΔH_f cannot be accurately calculated for a given compound, the relative values, and hence the BDE, are highly representative of the actual bond strengths. Therefore, the relative BDE of the different substrate–initiator bonds can accurately be calculated according to: ΔBDE=[BDE(substrate–**5**)] - [BDE(substrate–**6**)]. The calculated ΔBDE was 14 kJ/mol (gas phase), 46 kJ/mol (dichloromethane), and 120 kJ/ mol (water). The theoretical calculations confirmed the substrate–**5** bond is indeed stronger than the corresponding substrate–**6** bond, especially in water.

.

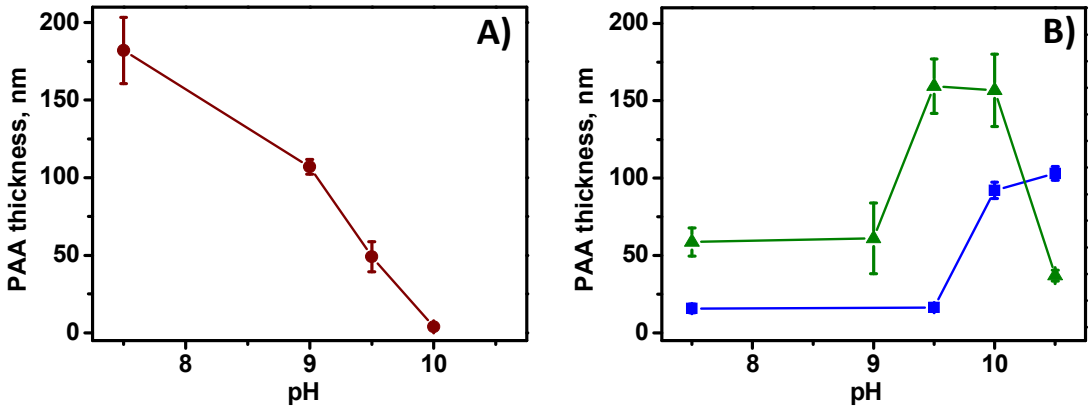

Figure 6. A) Variation of the PAA layer thickness grafted from initiator **6** at different pH without added salt. The pH was increased from 7.5 to 10.0. Original dry PAA thickness=120 nm. B) Variation of PAA layer thickness prepared from immobilized **5** at different pH without (squares) and with 10 mM NaCl (triangles). The sample was exposed to salt-free buffer solutions, where the pH increased from 7.5 to 10.5. Then, the sample was soaked in milliQ water overnight and exposed to buffer solutions from pH from 7.5 to 10.5 with 10 mM NaCl. Original dry PAA thickness=20 nm. All thickness measurements were done *in situ* using the AFM step-height method.

Surface forces characterization.

Normal and friction forces between two PAA layers of mica immobilized-**5** were measured using SFA under different pH and ionic strength. This was to assess the adhesion, friction and resistance to compression and shear of the polyelectrolyte brushes. The force profiles were measured step-wise during both approach and separation and each separation distance was

measured at equilibrium. This was taken at a distance variation of less than 0.5 nm/min. Measurements were done on five different pairs of PAA coated mica surfaces and they were reproduced on different contact positions with the same pair of surfaces. A wait time of 2 hours was set between each approach-separation cycle. The friction forces were measured at different separation distances ranging from large distances (corresponding to a negligible applied normal load) to smaller distances, corresponding to pressure of ca 40 atm for all pairs of surfaces. As for the force profiles, the lateral motion was initiated once the variation in the separation distance was less than 0.5 nm/min. The reported friction forces, F_s, are the average kinetic forces measured in the steady-state conditions (i.e., constant driving velocity and friction forces). The reported measurements were done at a sliding velocity of 1 μm/s for comparison with previously reported results. All reported friction forces were measured in the absence of surface damage, confirmed by the direct visualization of the contact region with the optical interferometry technique used for force measurements.

Figure 7 shows the measured normal force profiles in water at 25 °C for different pH (5.5 and 9.5) and salt concentrations (0 and 10 mM NaCl) between two PAA layers on mica prepared from immobilized-**5**. For given pH and salt concentration, the force profiles were not systematically reproducible and they exhibited hysteresis. These results suggest significant surface heterogeneity and thickness variability between the pairs analyzed. This most likely is from slight variances in the different degrees of polymerization[53, 54] and polydispersities[55] of the brushes between different samples, even when polymerized in the same reactor using identical polymerization conditions.[9, 56] The variable polydispersity of the polymer brushes are confirmed by AFM surface roughness measurements. The film roughness (rms) of PAA polymerized from

mica immobilized-**5** ranged from 1.3 to 2.3 nm (Table S1). This is much rougher than previously reported *grafted-to* PAA brushes whose surface roughness was 0.5 nm.[50] The rough film polymerized from the immobilized-**5** suggests that the polymer molecular weight and/or grafting density are not well controlled with *grafted-from*. Therefore, the polymer's structural changes in response to its surroundings cannot be accurately quantified. Nevertheless, the on-approach and separation force profiles measured are typical of those for polymer brushes. Only the on-approach measured surface profiles are illustrated for clarity. It should be noted that the force profiles do not clearly exhibit the long-rang exponential decay that is characteristic of double-layer electrostatic interactions. This would suggest that onset of the repulsion corresponds to the initial compression of the two apposing brush layers (i.e. twice the non-perturbed brush thickness). Half the onset distances for the mica immobilized PAA range between 50 and 225 nm is significantly larger than the measured AFM step-heights for the corresponding silica immobilized PAA of ca 20-160 nm (Fig. 6B). This can be explained by the two different approaches used to determine thickness with both instruments, AFM and SFA. The AFM thickness (or step-height) was determined using contact mode, which does not exclude the compression of the brushes. With SFA, the thickness was inferred from the range of the repulsive forces which is sensitive to the non-compressed outer most segments of the brushes. In addition, the long-ranged repulsive forces may also include some non-contact electrostatic effects. Therefore, it is expected to measure a larger thickness by the non-compressed SFA compared to AFM.

The relationships between the friction force (F_S) and the normal load (F_N) for three different experimental conditions with and without added salt are depicted in Figure 8. As can be seen from the normal forces profiles, the responsiveness of the brush to changes in pH and ionic

strength cannot be unequivocally identified from the F_S measurements (Figure 8). The F_S versus F_N curves are delimited by two linear curves, which set the limiting values of the friction coefficient. The friction coefficients range from ca 0.4 to 1.1 in salt-free water and increase to a maximum value of 3.9 with added salt. The values are relatively high compared to those previously measured between two *grafted-to* PAA brushes under similar experimental conditions.[50] The measured friction coefficients are more consistent with those measured by AFM for poly(2-(dimethylamino)ethyl methacrylate) brushes *grafted-from* gold.[51] The different friction coefficients for the *grafted-to* and *grafted-from* PAA brushes are most probably due to variations in the surface roughness, where the rms of *grafted*-from PAA in water was 1.3 as opposed to 0.4 for the *grafted-to* PAA. This is based on the well-known fact that the surface roughness has a significant effect on the friction coefficient, where it increases with surface roughness.[57,58] It is worthy to note that although high friction coefficients were obtained, the surfaces were not damaged during the force analyses. No surface damage was observed even under applied loads up to 20 mN/m, corresponding to pressures of ca 40 atm. This confirms the strong covalent attachment of the organophosphonic acid to the mica substrate and illustrates the suitability of this anchoring group as a robust alternative to siloxanes.

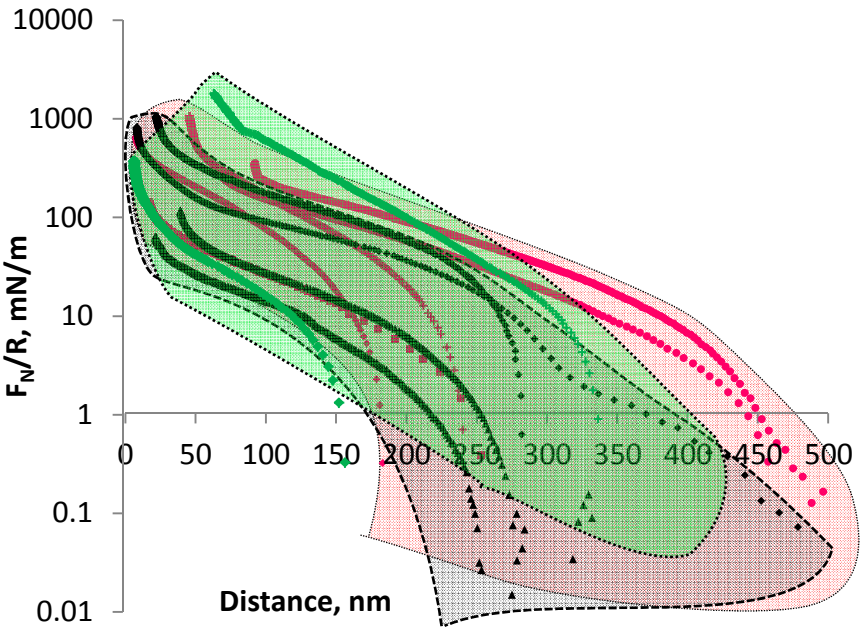

Figure 7. Normalized force profiles measured on approaching two opposing PAA brushes across (pink) water, (green) buffer solution pH 9.5 without salt and (gray) buffer solution pH 9.5 with salt. The shade areas represent the variability in the measured force profiles and the most representative profiles are illustrated. The PAA brushes were prepared on five mica pairs obtained from three independents experiments. (■) sample 1, (●) sample 2, (▲) sample 3 (◆) sample 4 and (+) sample 5.

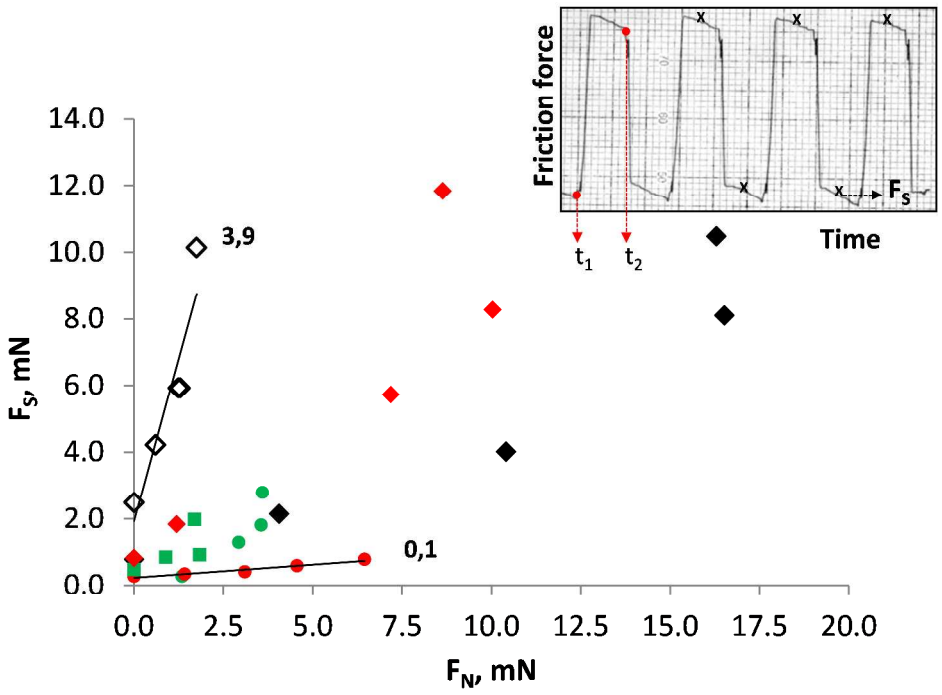

Figure 8. Friction force, F_S, as a function of the normal force, F_N, between two opposing PAA brushes measured in water (red symbols), buffer solution pH 9.5 without salt (green symbols) and buffer solution pH 9.5 with 10 mM salt (black symbols). Sample 1 (■), sample 2 (●), and sample 4 different spots (◆, ◇). All measurements were done at a sliding velocity of 1μm/s. Inset: typical friction traces. t_1 and t_2 illustrate times where sliding direction was reversed.

Conclusion

An organophosphonic acid (**5**) was investigated as an alternative to commonly used organosiloxanes for robustly immobilizing an ATRP initiator to silica and mica. Covalent attachment of a monolayer of **5** to both mica and silica substrates was possible. We demonstrated for the first time that the covalently grafted **5** to silica underwent surface polymerization of NaPAA and KPSPMAA via water-mediated ATRP to afford polyelectrolyte brushes. The swelling behavior of the resulting grafted PAA brushes and their resistance to

cleavage from the substrate at pH<10.5 demonstrated the robustness of the **5**–substrate bond. The robustness of the **5**–mica bond was further illustrated by surface force measurements, where PAA brushes resisted shearing and compression upwards of several atmospheres. It was successfully proven that organophosphonic acids are viable alternatives to siloxanes derivatives for the robust covalent attachment of ATRP initiators to silica surfaces. **5** is an attractive anchor for preparing covalently immobilized responsive smart materials that can sustain a wide range of environmental conditions. Meanwhile, SFA measurements demonstrated the complexity of controlling the thickness and surface homogeneity of PAA brushes prepared from water-mediated ATRP. The polydispersity and molecular weight of the polyelectrolytes *grafted-from* **5**-substrates are important parameters that need to be examined in more detail because they affect the surface roughness of the polymer film and the brush surface properties.

Acknowledgements. Financial support from the Natural Sciences and Engineering Research Council of Canada and Fondation Québécoise pour la Recherche en Nature et Technologies are acknowledged. Canadian Foundation for Innovation is also acknowledged for additional equipment and infrastructures. The Center for Self-Assembled Chemical Structures is also acknowledged. The authors thank Prof. C. Pellerin and Ms. M. Richard-Lacroix for access to the ATR-FTIR instrument and measurements, respectively. AIST NT and Mr. A. Krayev are also acknowledged for high resolution AFM images of the **5**-modified substrates.

References

1. A. J. Morse, S. Edmondson, D. Dupin, S. P. Armes, Z. Zhang, G. J. Leggett, R. L. Thompson and A. L. Lewis, *Soft Matter*, 2010, **6**, 1571-1579.
2. U. Raviv, S. Giasson, N. Kampf, J.-F. Gohy, R. Jérôme and J. Klein, *Nature*, 2003, **425**, 163-165.
3. O. Azzaroni, *J. Polym. Sci. Pol. Chem.*, 2012, **50**, 3225-3258.
4. P. G. Degennes, *Macromolecules*, 1980, **13**, 1069-1075.
5. S. Minko, *Polym. Rev.*, 2006, **46**, 397-420.
6. R. Barbey, L. Lavanant, D. Paripovic, N. Schuwer, C. Sugnaux, S. Tugulu and H. A. Klok, *Chem. Rev.*, 2009, **109**, 5437-5527.
7. C. M. Hui, J. Pietrasik, M. Schmitt, C. Mahoney, J. Choi, M. R. Bockstaller and K. Matyjaszewski, *Chem. Mater.*, 2013.
8. I. Tokarev, M. Motornov and S. Minko, *J. of Mater. Chem.*, 2009, **19**, 6932-6948.
9. Y. Tsujii, K. Ohno, S. Yamamoto, A. Goto and T. Fukuda, *Adv. Polym. Sci.*, 2006, **197**, 1-45.
10. R. Barbey, L. Lavanant, D. Paripovic, N. Schuwer, C. Sugnaux, S. Tugulu and H. A. Klok, *Chem. Rev.*, 2009, **109**, 5437-5527.
11. C. P. Tripp and M. L. Hair, *J. Phys. Chem.*, 1993, **97**, 5693-5698.
12. D. K. Schwartz, *Annu. Rev.of Phys, Chem.*, 2001, **52**, 107-137.
13. X. L. Zhao and R. Kopelman, *J. of Phys. Chem.*, 1996, **100**, 11014-11018.
14. O. Borozenko, R. Godin, K. L. Lau, W. Mah, G. Cosa, W. G. Skene and S. Giasson, *Macromolecules*, 2011, **44**, 8177-8184.
15. O. Borozenko, C. Ou, W. G. Skene and S. Giasson, *Polym. Chem.*, 2013.

16. P. J. Hotchkiss, S. C. Jones, S. A. Paniagua, A. Sharma, B. Kippelen, N. R. Armstrong and S. R. Marder, *Acc. Chem. Res.*, 2012, **45**, 337-346.

17. S. A. Paniagua, P. J. Hotchkiss, S. C. Jones, S. R. Marder, A. Mudalige, F. S. Marrikar, J. E. Pemberton and N. R. Armstrong, *J. Phys. Chem. C*, 2008, **112**, 7809-7817.

18. C. Queffelec, M. Petit, P. Janvier, D. A. Knight and B. Bujoli, *Chem. Rev.*, 2012, **112**, 3777-3807.

19. B. M. Silverman, K. A. Wieghaus and J. Schwartz, *Langmuir*, 2005, **21**, 225-228.

20. A. Cattani-Scholz, D. Pedone, M. Dubey, S. Neppl, B. Nickel, P. Feulner, J. Schwartz, G. Abstreiter and M. Tornow, *ACS Nano*, 2008, **2**, 1653-1660.

21. K. S. Midwood, M. D. Carolus, M. P. Danahy, J. E. Schwarzbauer and J. Schwartz, *Langmuir*, 2004, **20**, 5501-5505.

22. A. Cattani-Scholz, D. Pedone, F. Blobner, G. Abstreiter, J. Schwartz, M. Tornow and L. Andruzzi, *Biomacromolecules*, 2009, **10**, 489-496.

23. K. C. Liao, A. G. Ismail, L. Kreplak, J. Schwartz and I. G. Hill, *Adv. Mater.*, 2010, **22**, 3081-3085.

24. J. E. McDermott, M. McDowell, I. G. Hill, J. Hwang, A. Kahn, S. L. Bernasek and J. Schwartz, *J. of Phys. Chem.A*, 2007, **111**, 12333-12338.

25. M. McDowell, I. G. Hill, J. E. McDermott, S. L. Bernasek and J. Schwartz, *App.Phys.Lett.*, 2006, **88**.

26. A. Bora, A. Pathak, K. C. Liao, M. I. Vexler, A. Kuligk, A. Cattani-Scholz, B. Meinerzhagen, G. Abstreiter, J. Schwartz and M. Tornow, *App. Phys. Lett.*, 2013, **102**.

27. I. Minet, J. Delhalle, L. Hevesi and Z. Mekhalif, *J. Colloid Interface Sci.*, 2009, **332**, 317-326.

28. B. Barthelemy, S. Devillers, I. Minet, J. Delhalle and Z. Mekhalif, *J. Colloid Interface Sci.*, 2011, **354**, 873-879.
29. K. Babu and R. Dhamodharan, *Nanoscale Res. Lett.*, 2008, **3**, 109-117.
30. S. Devillers, B. Barthelemy, J. Delhalle and Z. Mekhalif, *ACS Appl. Mater. Interfaces*, 2011, **3**, 4059-4066.
31. B. Barthelemy, S. Devillers, I. Minet, J. Delhalle and Z. Mekhalif, *Appl. Surf. Sci.*, 2011, **258**, 466-473.
32. M. Chen, W. H. Briscoe, S. P. Armes, H. Cohen and J. Klein, *ChemPhysChem*, 2007, **8**, 1303-1306.
33. U. Raviv, J. Frey, R. Sak, P. Laurat, R. Tadmor and J. Klein, *Langmuir*, 2002, **18**, 7482-7495.
34. P. A. Schorr, T. C. B. Kwan, S. M. Kilbey, E. S. G. Shaqfeh and M. Tirrell, *Macromolecules*, 2002, **36**, 389-398.
35. N. V. Tsarevsky and K. Matyjaszewski, *Chem. Rev.*, 2007, **107**, 2270-2299.
36. B. Lego, W. G. Skene and S. Giasson, *Langmuir*, 2008, **24**, 379-382.
37. B. Liberelle, X. Banquy and S. Giasson, *Langmuir*, 2008, **24**, 3280-3288.
38. J. Israelachvili, *J. Colloid Interface Sci.*, 1973, **44**, 259-272.
39. J. N. Israelachvili and G. E. Adams, *J. Chem. Soc. Faraday Trans.*, 1978, **74**, 975-&.
40. J. N. Israelachvili, P. M. Mcguiggan and A. M. Homola, *Science*, 1988, **240**, 189-191.
41. G. Luengo, F.-J. Schmitt, R. Hill and J. Israelachvili, *Macromolecules*, 1997, **30**, 2482-2494.
42. E. L. Hanson, J. Schwartz, B. Nickel, N. Koch and M. F. Danisman, *J. Am. Chem. Soc.*, 2003, **125**, 16074-16080.

43. J. T. Woodward, A. Ulman and D. K. Schwartz, *Langmuir*, 1996, **12**, 3626-3629.

44. R. C. Longo, K. Cho, W. G. Schmidt, Y. J. Chabal and P. Thissen, *Adv. Funct. Mater.*, 2013, **23**, 3471-3477.

45. R. Quinones, A. Raman and E. S. Gawalt, *Thin Solid Films*, 2008, **516**, 8774-8781.

46. D. L. Allara and R. G. Nuzzo, *Langmuir*, 1985, **1**, 45-52.

47. D. L. Allara and R. G. Nuzzo, *Langmuir*, 1985, **1**, 52-66.

48. B. Lego, W. G. Skene and S. Giasson, *Macromolecules*, 2010, **43**, 4384-4393.

49. H. H. Anderson, *Inorg. Chem.*, 1964, **3**, 108-109.

50. B. Liberelle and S. Giasson, *Langmuir*, 2008, **24**, 1550-1559.

51. N. Nordgren and M. W. Rutland, *Nano Letters*, 2009, **9**, 2984-2990.

52. E. B. Zhulina, T. M. Birshtein and O. V. Borisov, *Macromolecules*, 1995, **28**, 1491-1499.

53. D. M. Jones, A. A. Brown and W. T. S. Huck, *Langmuir*, 2002, **18**, 1265-1269.

54. J. N. Kizhakkedathu, R. Norris-Jones and D. E. Brooks, *Macromolecules*, 2004, **37**, 734-743.

55. N. V. Tsarevsky, W. A. Braunecker, S. J. Brooks and K. Matyjaszewski, *Macromolecules*, 2006, **39**, 6817-6824.

56. K. Matyjaszewski, *Prog. Polym. Sci.*, 2005, **30**, 858-875.

57. J. Stiernstedt, N. Nordgren, L. Wågberg, H. Brumer Iii, D. G. Gray and M. W. Rutland, *J. Colloid Interface Sci.*, 2006, **303**, 117-123.

58. X. Banquy, X. X. Zhu and S. Giasson, *J. Phys. Chem. B*, 2008, **112**, 12208-12216.